PNAS RESEARCH ARTICLE | BIOPHYSICS AND COMPUTATIONAL BIOLOGY

Vimentin promotes actin assembly by stabilizing ATP-actin subunits at the barbed end

Lilian Paty[a], Lukas Kalvoda[b], Maritzaida Varela-Salgado[a], Quang D. Tran[a,1], Martin Lenz[b,c], Antoine Jégou[a,2], Guillaume Romet-Lemonne[a,2], and Cécile Leduc[a,2]

Affiliations are included on p. 10.

Edited by Thomas D. Pollard, Yale University, New Haven, CT; received November 12, 2025; accepted May 28, 2026

Vimentin intermediate filaments play essential roles in maintaining cell integrity and regulating numerous cellular functions. In particular, vimentin cooperates with the actin cytoskeleton in key cellular processes that rely on actin dynamics, such as migration, division, and mechanosensing. While there is evidence that these two cytoskeletal components interact in cells, the underlying molecular mechanisms are only partially understood. Actin and vimentin can interact through biochemical signaling pathways or via cross-linkers, but whether they engage in a direct protein–protein interaction has remained controversial, in part because such interactions are difficult to isolate and characterize in cells. Using in vitro reconstitution coupled to theoretical modeling, and total internal reflection fluorescence microscopy to monitor the elongation of single actin filaments, we show that vimentin promotes actin elongation by stabilizing actin subunits at the barbed end in a dose-dependent manner. Strikingly, this effect depends on the nucleotide state of actin, as the acceleration is only observed for the elongation from adenosine triphosphate (ATP)-actin, and not adenosine diphosphate (ADP)-actin monomers. We further establish that neither the vimentin tail nor head domains are required for this effect, and both filamentous and nonfilamentous vimentin enhance actin elongation. Finally, we find that vimentin promotes the nucleation of actin filaments. Consistently, magnetic pull-down assays demonstrate a direct interaction between vimentin and ATP-actin monomers. Altogether, these findings identify vimentin as an unexpected new actor in the regulation of actin dynamics at the barbed end and bring new insights into the functional role of vimentin through cytoskeletal crosstalk.

cytoskeleton | intermediate filaments | assembly dynamics | cytoskeletal crosstalk | in vitro reconstitution

Significance

The cytoskeleton is composed of three types of filaments: actin, microtubules, and intermediate filaments, which coordinate to control cell shape, mechanics, and movement. Among them, the contribution of vimentin intermediate filaments to these functions has remained elusive. While studies highlighted their influence on actin dynamics, the underlying molecular mechanisms remain to be determined. Using in vitro reconstitution from purified proteins, we show that vimentin directly promotes actin filament assembly by selectively stabilizing ATP-actin subunits at the fast-growing end. This mechanism, distinct from that of canonical actin regulators, reveals a previously unrecognized mode of cytoskeletal regulation. Our findings identify vimentin as an unexpected modulator of actin dynamics, providing a molecular understanding of how intermediate filaments contribute to cytoskeletal organization.

The cytoskeleton is a dynamic network of three interconnected filament systems: actin filaments, microtubules, and intermediate filaments, that allow cells to shape and organize themselves in space and time while mechanically engaging with their environment. Intermediate filaments are composed of a large family of proteins whose expression levels are cell- and tissue-type specific (1–4). Among them, vimentin is expressed in mesenchymal cells and widely used as a marker of the epithelial-to-mesenchymal transition, during which epithelial cells acquire migratory and invasive properties (5, 6). Unlike actin and microtubules, which rapidly remodel through active turnover, vimentin self-assembles into long-lived apolar filaments (3, 7–9), yet is involved in highly dynamic processes such as migration, division, and mechanosensing (4, 10–13). Growing evidence suggests that vimentin contributes to these functions through its crosstalk with the other cytoskeletal filaments (2, 14–16), including actin (17). Early studies showed that vimentin-deficient cells exhibit reduced acto-myosin contractility (12). More recent work revealed that vimentin coordinates actin stress fiber assembly (18–20), orients traction forces that drive migration (21), and tunes cell stress by assisting in actomyosin-based force transmission (10). There is also a mechanical synergy between the two types of filaments (22), which is crucial for maintaining cell integrity (23). The actin–vimentin interplay likely relies on reciprocal regulation of filament organization and dynamics, with vimentin modulating actin in both nondividing (18, 24–26) and dividing cells (11, 13) and actin in turn influencing vimentin (18, 27–29). This interplay is mediated through indirect biochemical signaling, direct interactions, or interactions via crosslinkers (2, 14, 18, 30–33), but the precise molecular mechanisms remain to be fully elucidated.

In vitro reconstitution with purified proteins provides a powerful approach to dissect how actin and vimentin coordinate their activities, as it can disentangle their interactions from the complexity of the cellular environment. Bulk rheology studies of actin–vimentin networks have suggested that the observed viscoelastic properties of the composite

The authors declare no competing interest.

This article is a PNAS Direct Submission.

Copyright © 2026 the Author(s). Published by PNAS. This article is distributed under Creative Commons Attribution-NonCommercial-NoDerivatives License 4.0 (CC BY-NC-ND).

[1]Present address: Department of Physiology and Biomedical Engineering, Mayo Clinic, Rochester, MN 55905.

[2]To whom correspondence may be addressed. Email: antoine.jegou@ijm.fr, romet@ijm.fr, or cecile.leduc@ijm.fr.

This article contains supporting information online at https://www.pnas.org/lookup/suppl/doi:10.1073/pnas.2531232123/-/DCSupplemental.

Published July 6, 2026.

Downloaded from https://www.pnas.org by Cecile Leduc on July 6, 2026 from IP address 81.194.28.6.

networks cannot be explained without direct actin–vimentin interactions (34, 35), and that vimentin's tail domain is implicated in the interaction (34). However, another study has argued that the mechanics of composite networks could be explained solely by the additive properties of their individual components, without requiring direct filament–filament binding (36). More recently, single-filament imaging found no evidence for actin–vimentin filament coalignment, suggesting that if there is an interaction between the filaments, it must be transient and weak (37). Thus, whether actin and vimentin interact directly, and how such interactions might influence filament dynamics, remains unresolved. Understanding the effect of vimentin on actin filaments alone in simplified in vitro systems is necessary, before adding more components, such as crosslinkers and regulatory proteins, in more complex bottom–up approaches that would come closer to the cellular context.

Here, using an actin single-filament assay coupled to theoretical modeling, we found that vimentin directly promotes actin filament nucleation and elongation. We show that the molecular mechanism responsible for the enhanced elongation involves vimentin stabilizing actin subunits at the barbed end in a nucleotide state-dependent manner. These findings reveal a previously unrecognized role for vimentin as a regulator of actin filament growth, highlighting a direct interaction through which vimentin intermediate filaments can influence actin dynamics.

Results

Vimentin Promotes Actin Filament Elongation at the Barbed End. In order to assess the impact of vimentin on actin assembly dynamics, we used an assay that allows direct visualization of actin elongation at the single filament level using time-lapse Total Internal Reflection Fluorescence (TIRF) microscopy, hereinafter referred to as "actin polymerization assay" (Fig. 1*A*). Small prepolymerized biotinylated fragments of actin filaments (F-actin) (Fig. 1*A*, magenta) were first anchored to a passivated glass surface coated with neutravidin. Upon addition of 0.5 µM of actin monomers in the ATP-bound state (ATP-G-actin, 10% fluorescently labeled), with a low fraction of biotinylation (~0.15%), filaments elongated at their fast-growing barbed-end with sparse anchoring points along their length (~0.5 anchors per µm) (Fig. 1 *A* and *B*, yellow). At this actin concentration, the elongation of the pointed end is negligible over the time scale of the experiments. This low biotinylation level minimized potential effects on elongation while maintaining sufficient proximity to the surface for automated filament tracking. Actin filament elongation was monitored in either assembly buffer alone (control) or buffer containing 18 µM of vimentin (1 mg/mL) preassembled into filaments. Automated filament tracking and systematic quantification of the elongation rate (Fig. 1*C*) demonstrated that actin filaments elongated faster in the presence of vimentin filaments than in the control condition (Fig. 1*D*). This effect was consistently reproducible across repeated experiments (4.5 ± 0.7 sub/s with vimentin vs. 3.8 ± 0.6 sub/s without vimentin, mean ± SD, N = 11 independent replicates), and robust with salinity (*SI Appendix,* Fig. S1). Control experiments verified that the actin elongation rates with low biotinylation were comparable to those without anchoring points, using methylcellulose to confine the filaments (*SI Appendix,* Fig. S2*A*). Moreover, we verified that vimentin's effect on actin elongation was similar in both anchoring and methylcellulose conditions (*SI Appendix,* Fig. S2*B*). However, because methylcellulose induces actin–vimentin coalignment (potentially bundling them through depletion effects), as observed when a small fraction of vimentin was fluorescently labeled within the network (*SI Appendix,* Fig. S2*C*), we rather used sparse anchoring to confine the filaments on the surface. Because, in cells, actin monomers are bound to profilin and F-actin elongate from profilin–G-actin complexes, we verified that vimentin also promoted elongation from profilin–G-actin (*SI Appendix,* Fig. S3 *A-B*). These results demonstrate that the sole presence of vimentin filaments is sufficient to accelerate actin elongation in the absence of any actin–vimentin crosslinkers.

Vimentin Promotes Actin Elongation by Preventing the Departure of ATP-Actin Subunits. The net elongation rate of actin filaments at the barbed end reflects the result of actin monomer association and dissociation events. To gain insights into the mechanism by which vimentin accelerates actin elongation, we sought to determine how the arrival and the departure of monomers at the barbed end were respectively affected by vimentin. To do so, we repeated the actin polymerization assay at different ATP-G-actin concentrations (Fig. 1*E*). The elongation rates displayed an affine relationship with the ATP-G-actin concentration, allowing the extraction of the on-rate (slope) and the off-rate (intercept) constants, called k_{on}^{ATP} and k_{off}^{ATP} respectively (Fig. 1*F*). Strikingly, we observed that vimentin reduced the actin off-rate constant close to zero (0.3 ± 0.3 s^{-1} with vimentin vs. 0.9 ± 0.3 s^{-1} in the control condition, mean ± SD, $N = 3$ independent experiments), while having no significant effect on the on-rate constant (11.6 ± 1.3 μM^{-1} s^{-1} with vimentin vs. 11.0 ± 1.4 μM^{-1} s^{-1} in the control condition, mean ± SD, $N = 3$ independent experiments), consistent with the absence of any effect of vimentin on actin monomer diffusion (*SI Appendix,* Fig. S4). Although a minor effect on the on-rate may exist, the dominant effect is on the off-rate. Thus, vimentin accelerates actin elongation by stabilizing monomers at the growing barbed end rather than increasing the monomer binding rate (Fig. 1*G*).

Vimentin Does Not Stabilize Actin Filaments against Depolymerization. The stabilization of ATP-actin subunits at the barbed end induced by vimentin during polymerization led us to test whether vimentin could also protect actin filaments from depolymerization. We performed an actin depolymerization assay where nonbiotinylated actin filaments were first polymerized from surface-anchored spectrin-actin seeds. Then, unpolymerized actin monomers were washed out, and filament depolymerization was monitored using methylcellulose to keep the filaments close to the surface (Fig. 2*A*). The presence of vimentin did not decrease the actin depolymerization rate (3.7 ± 0.8 sub/s with vimentin vs. 3.4 ± 0.7 sub/s without vimentin, mean ± SD, $N = 4$ independent replicates), indicating that vimentin stabilizes the barbed end only when the actin filament is growing (Fig. 2*A*). On the contrary, we observed a mild increase in the depolymerization rate. This surprising result might be explained by the difference in state of the barbed end under polymerizing and depolymerizing conditions. Upon incorporation into a filament, the conformational change of the subunits triggers the ATP hydrolysis to ADP.Pi within seconds, and the inorganic phosphate is then released with a half-time of a few minutes (39–41). Actin subunits can thus exist under three different nucleotide states (ATP-, ADP.Pi-, and ADP-actin) within the filament. In polymerizing conditions, when the polymerization rate is faster than the ATP hydrolysis rate [0.3 s^{-1} (42)], the barbed end is mostly occupied by ATP-actin subunits, and the off-rate measured indirectly corresponds to the dissociation of ATP-actin subunits (k_{off}^{ATP}, Fig. 1*G*). In contrast, in the depolymerization assay, we monitor the disassembly of ADP/ADP.Pi-actin subunits

Downloaded from https://www.pnas.org by Cecile Leduc on July 6, 2026 from IP address 81.194.28.6.

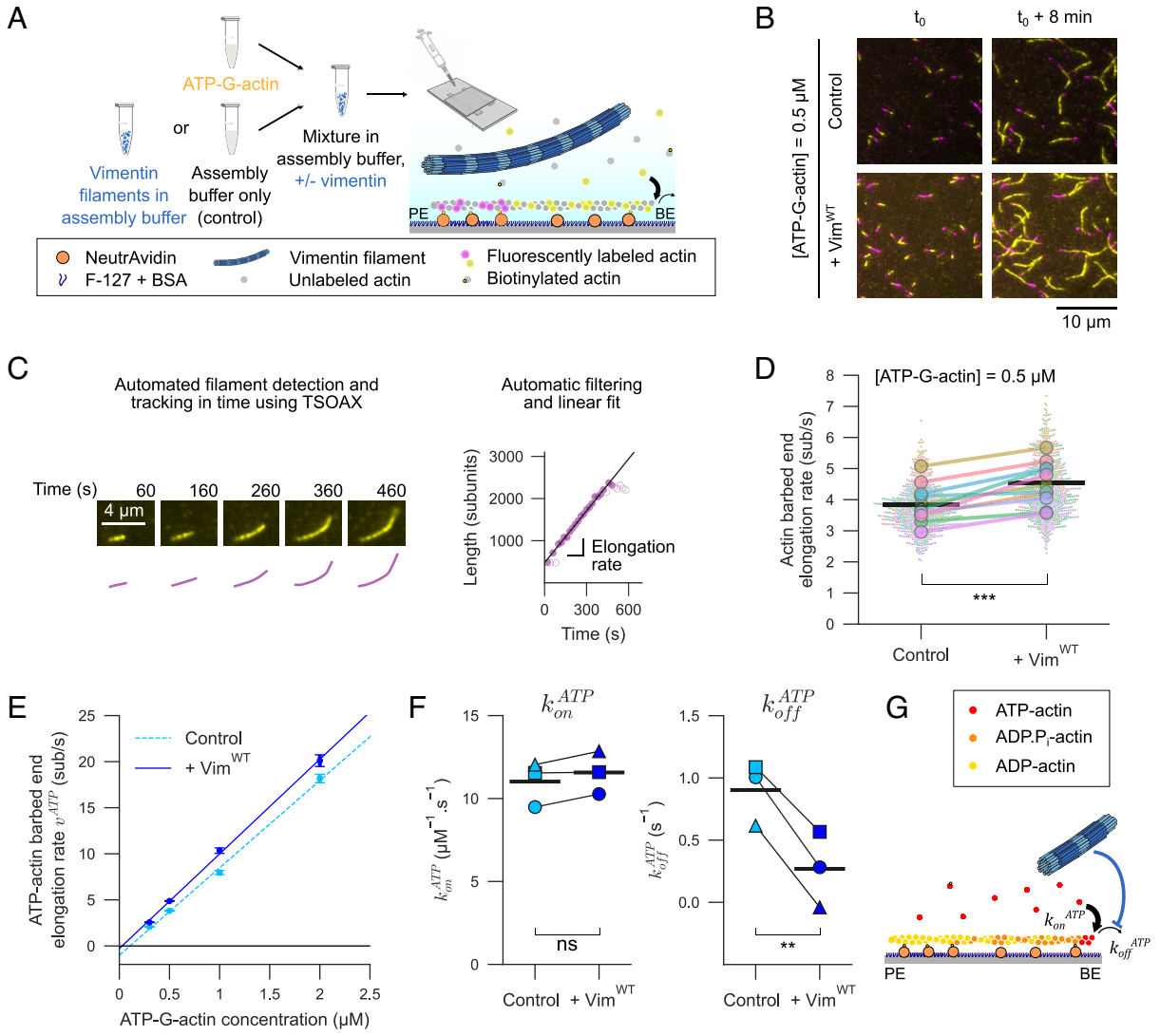


Fig. 1. Vimentin promotes actin filament elongation at the barbed end by stabilizing ATP-actin subunits. (*A*) Actin polymerization assay. Fragments of actin filaments (10% Atto-643, 10% biotin labeled, magenta) were prepolymerized for ≥1 h at 10 µM by adding 100 mM KCl to the ATP-G-actin solution in G-buffer, then diluted and fragmented by pipetting and introduced in a flow chamber that was functionalized with neutrAvidin and passivated by F127 and BSA. ATP-G-actin (10% AF-488 or Atto-488, 0.15% biotin labeled, yellow) was mixed at a concentration of 0.5 µM in assembly buffer (10 mM HEPES pH 7.0, 1 mM sodium phosphate, 1 mM $MgCl_2$, 0.2 mM EGTA, 100 mM KCl) only (Control) or in buffer with 18 µM of unlabeled wild-type vimentin (1 mg/mL) preassembled into filaments. This solution was then introduced in the flow chamber, and actin monomers assembled from the barbed end of the anchored F-actin fragments in the presence or absence of vimentin (blue). Actin filament elongation was monitored by TIRF microscopy. PE: pointed end, BE: barbed end. (*B*) Representative TIRF snapshots of actin filaments polymerizing without (Control) or with (+Vim^{WT}) 18 µM vimentin preassembled into filaments. (*C*) Method used to quantify the actin barbed end elongation rate. (*Left*) Example of TIRF time-lapse sequence of an elongating filament, along with the corresponding segmentation by the software TSOAX (38). (*Right*) Length in subunits of this actin filament as a function of time. The elongation rate was quantified by automatic filtering of detection errors (open circles) and linear fitting. Detection errors are due to the sparse anchoring of the filament: Between two anchoring points, the filament can sometimes grow out-of-plane, leading to a low TIRF signal and an underestimation of its length. (*D*) Actin barbed end elongation rate (subunits per second) in the absence (Control) or in the presence (+Vim^{WT}) of 18 µM vimentin preassembled into filaments. Colors depict experiments performed on the same day—these experiments were paired to account for day-to-day variability. Small dots: individual actin filament elongation rates ($n \geq 20$ rates per experiment), large dots: average elongation rates of the replicates ($N = 11$ independent replicates), black bars: mean elongation rate computed from the replicate averages. Statistical significance of the difference was evaluated by running a two-tailed paired *t* test over the replicate averages. ***$P < 0.001$. (*E*) Actin barbed end elongation rate as a function of ATP-G-actin concentration in the absence (Control, light blue) or in the presence of 18 µM of vimentin (1 mg/mL) assembled into filaments (+Vim^{WT}, dark blue). Data are shown as the mean ± SEM for $n \geq 20$ rates per condition. Dashed and solid lines represent linear fits of the means to the equation $v_{ATP} = k_{on}^{ATP}$ [ATP-G-actin]$- k_{off}^{ATP}$, to extract the on- and off-rate constants k_{on}^{ATP} and k_{off}^{ATP}. Experiments were conducted in the standard assembly buffer at 50 mM KCl. (*F*) Quantification of the ATP-actin on- and off-rate constants at the barbed end k_{on}^{ATP} and k_{off}^{ATP} extracted from $N = 3$ independent replicates (filled symbols) and mean rates (black bars), in the absence (Control, light blue) or in the presence of 18 µM of vimentin (1 mg/mL) assembled into filaments (+Vim^{WT}, dark blue). Statistical significance of the difference between conditions was evaluated by running two-tailed paired *t* tests over the replicate averages. **$P < 0.01$, ns: not significant ($P > 0.05$). (*G*) Schematics of the nucleotide states of actin in the standard actin polymerization assay. The barbed end (BE) is occupied by ATP-actin subunits (red), and free ATP-actin monomers in solution bind and unbind from the barbed end with rate constants k_{on}^{ATP} and k_{off}^{ATP}, respectively. Deeper within the filament, actin subunits exist as ADP.P_i-actin (orange) and ADP-actin (yellow). Vimentin (blue) increases the net ATP-actin elongation rate at the barbed end by decreasing the ATP-actin off-rate constant k_{off}^{ATP}.

Downloaded from https://www.pnas.org by Cecile Leduc on July 6, 2026 from IP address 81.194.28.6.

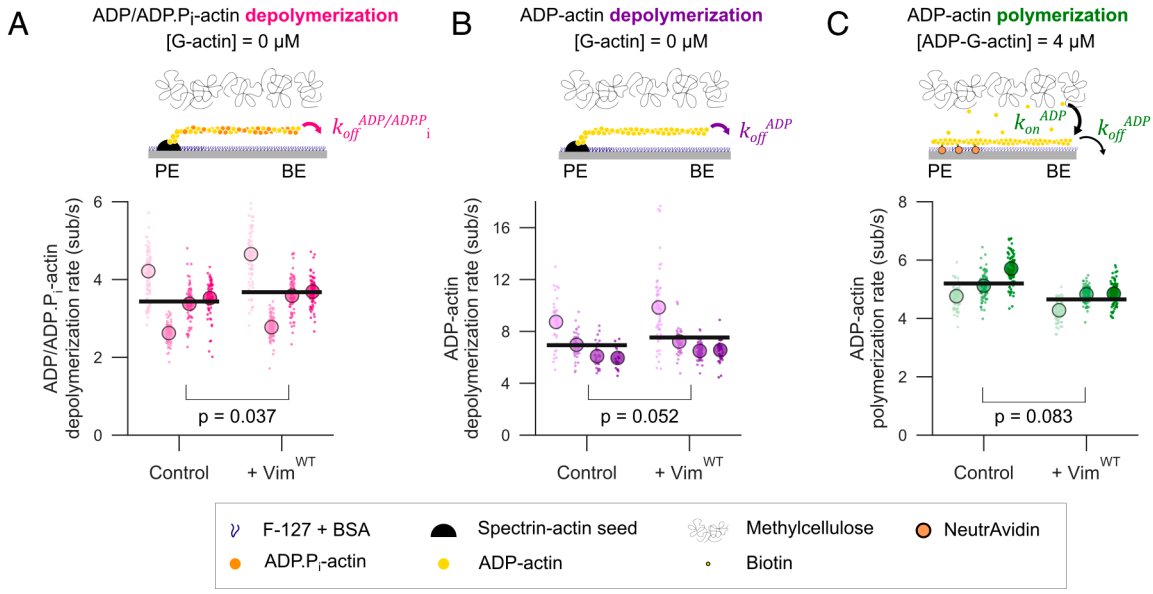


Fig. 2. Vimentin's stabilizing effect at the barbed end is nucleotide-dependent. (*A*, *Top*) Actin depolymerization assay in the standard assembly buffer (same as in Fig. 1), containing 1 mM sodium phosphate. Actin filaments were polymerized from spectrin-actin seeds by flowing ATP-actin monomers in the flow chamber. Nonpolymerized actin monomers were then rinsed, and the depolymerization of actin filaments was monitored by TIRF microscopy, keeping the filaments close to the surface using methylcellulose. As the assembly buffer contains 1 mM sodium phosphate, the depolymerization rate results from the off-rate constants of both ADP.Pi- and ADP-actin. (*Bottom*) ADP/ADP.P_i-actin depolymerization rate in the absence (Control) or in the presence (+Vim^{WT}) of 18 µM of vimentin (1 mg/mL) assembled into filaments. Small dots: individual depolymerization rates ($n \geq 20$ rates per replicate), large dots: average depolymerization rates of the replicates ($N = 4$ independent replicates), black bars: mean depolymerization rate computed from the replicate averages. (*B*, *Top*) Actin depolymerization assay in Tris assembly buffer (10 mM Tris-HCl, pH 7.5 at 25 °C, 1 mM $MgCl_2$, 0.2 mM EGTA, 50 mM KCl). Actin filaments were polymerized from spectrin-actin seeds by flowing ATP-actin monomers in the flow chamber. Nonpolymerized actin monomers were then rinsed. After waiting for 5 min for ATP to get hydrolyzed and inorganic phosphate to be released, the depolymerization of actin filaments was monitored by TIRF microscopy, keeping the filaments close to the surface using methylcellulose. (*Bottom*) ADP-actin depolymerization rate in the absence (Control) or in the presence (+Vim^{WT}) of 18 µM of vimentin (1 mg/mL) assembled into filaments. Small dots: individual depolymerization rates ($n \geq 20$ rates per replicate), large dots: average depolymerization rates of the replicates ($N = 4$ independent replicates), black bars: mean depolymerization rate computed from the replicate averages. (*C*, *Top*) ADP-actin polymerization assay in Tris assembly buffer. ADP-G-actin was obtained by incubating ATP-G-actin at 10 µM in ATP-free G-buffer supplemented with 2.5 mM glucose, 0.2 mM EGTA, 20 µM $MgCl_2$, and 15 U/mL hexokinase for 18 h on ice. Unlabeled ADP-G-actin was mixed with 50 nM Alexa488-labeled actin-binding domain of utrophin in Tris assembly buffer and introduced in a flow chamber to polymerize from anchored F-actin fragments. The ADP-G-actin concentration was 4 µM. The filaments were kept close to the surface by methylcellulose and their elongation was followed by TIRF microscopy. (*Bottom*) ADP-actin polymerization rate in the absence (Control) or in the presence (+Vim^{WT}) of 18 µM of vimentin (1 mg/mL) assembled into filaments. Small dots: individual polymerization rates ($n \geq 20$ rates per replicate), large dots: average polymerization rates of the replicates ($N = 3$ independent replicates), black bars: mean polymerization rate computed from the replicate averages. Statistical significance of the differences between conditions in *A*–*C* was evaluated by running two-tailed paired *t* tests over the replicate averages. In *A*–*C*, experiments were paired to account for day-to-day variability, and color shades denote paired and comparable experiments.

($k_{off}^{ADP/ADP.Pi}$, Fig. 2*A*). Indeed, the presence of 1 mM sodium phosphate in the buffer which comes with vimentin, prevents the full conversion to ADP-actin filaments by maintaining an equilibrium between filament-bound and soluble phosphate (*SI Appendix, Materials and Methods*). The fact that vimentin has no impact on ADP/ADP.Pi depolymerization suggests that its stabilizing action at the barbed end is specific to ATP-actin subunits.

Vimentin Stabilizes ATP-Actin, But Not ADP-Actin Monomers at the Barbed End. To assess the influence of the actin nucleotide state on the stabilizing effect of vimentin, we first repeated the depolymerization assay in a Tris buffer without phosphate (Fig. 2*B*). This allowed us to probe the impact of vimentin on the ADP-actin off-rate constant k_{off}^{ADP}. As observed in the phosphate-containing buffer, vimentin did not have a stabilizing effect on the barbed end (7.5 ± 1.6 sub/s with vimentin vs. 6.9 ± 1.3 sub/s without vimentin, mean ± SD, $N = 4$ independent replicates), suggesting that vimentin should not be able to accelerate actin filament elongation from ADP-G-actin. To verify this, we monitored actin polymerization from ADP-actin monomers (ADP-G-actin) by converting ATP-G-actin into ADP-G-actin prior to the assay (Fig. 2*C*). Because ADP-actin has a higher critical concentration than ATP-actin (39, 43, 44), we performed the actin polymerization assay at 4 µM ADP-G-actin instead of 0.5 µM, and in a Tris buffer without phosphate to avoid any conversion to ADP.Pi. However, this higher actin concentration increased the background signal when a small fraction of actin was fluorescently labeled, preventing accurate tracking of filament elongation. To overcome this constraint, we used a low concentration (50 nM) of a fluorescently labeled actin filament–binding domain from utrophin, which reliably reports filament length without interfering with assembly (45, 46) or with the effect of vimentin on actin elongation (*SI Appendix*, Fig. S5). Unlike with ATP-actin, we did not observe any acceleration of ADP-actin polymerization by vimentin (4.7 ± 0.3 sub/s with vimentin vs. 5.2 ± 0.5 sub/s without vimentin, mean ± SD, $N = 3$ independent replicates), confirming that the stabilizing effect of vimentin depends on the nucleotide state of the actin subunits and occurs only for ATP-actin. Taken together, these results demonstrate that vimentin can stabilize the barbed end of actin filaments when occupied by ATP-actin subunits, thereby enhancing polymerization. In contrast, when the barbed end is composed of ADP-actin subunits, vimentin has no stabilization effect, which explains the absence of an effect on actin depolymerization.

Nonfilamentous Vimentin Also Promotes Actin Elongation. We next asked whether vimentin's effect on actin elongation depends on vimentin's filament-forming capacity. In vimentin-expressing cells, vimentin is found as elongated filaments, short filaments also

Downloaded from https://www.pnas.org by Cecile Leduc on July 6, 2026 from IP address 81.194.28.6.

called squiggles, and tetramers (4, 47, 48). At low ionic strength, purified vimentin spontaneously self-assembles into tetramers (3, 49). By raising the ionic strength, tetramers associate laterally into short filaments known as unit-length filaments (ULFs), which subsequently anneal end-to-end to form longer filaments (3, 49). To arrest assembly at different stages, we produced different mutants of vimentin (Fig. 3*A*). The headless mutant ($Vim^{\Delta head}$), which lacks the N-terminal disordered head domain, forms tetramers but fails to laterally assemble into ULFs (49). The point-mutated vimentin Vim^{Y117L} forms ULFs that cannot anneal end-to-end to form longer filaments (50). Performing the actin polymerization assay (Fig. 1*A*) with these vimentin mutants revealed the same increase in actin elongation rate as observed with wild-type vimentin (Vim^{WT}), compared with the vimentin-free control condition (Fig. 3*B*). We conclude that the effect of vimentin on actin elongation can occur even with vimentin tetramers and does not require vimentin to be assembled into long filaments.

Vimentin's Disordered Tail Domain Is Not Required to Promote Actin Elongation. Because vimentin's disordered tail domain has been proposed to mediate a direct actin–vimentin interaction (34), we asked whether this domain is required for the acceleration of

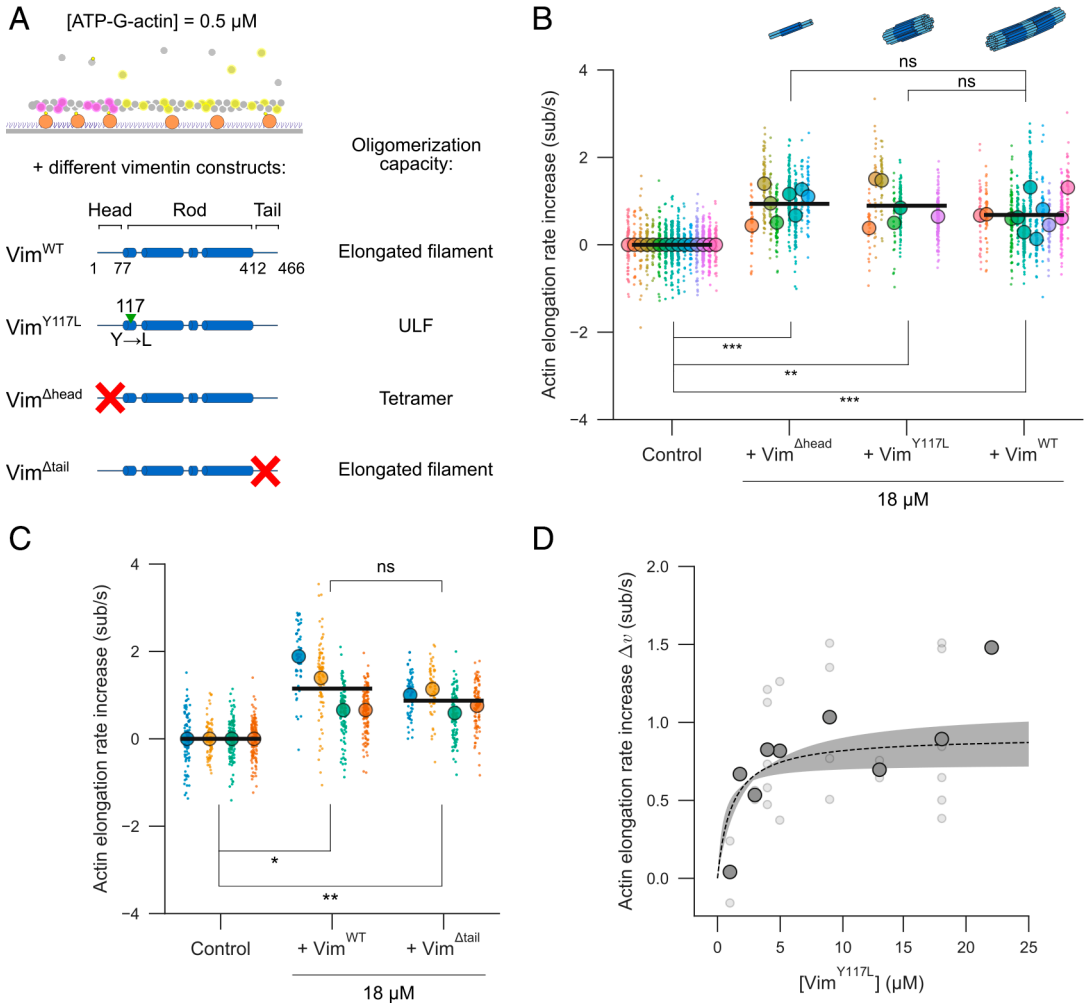


Fig. 3. Vimentin acceleration of actin elongation is independent of its oligomerization state and tail domain and is dose-dependent. (*A*) The actin polymerization assay (at 0.5 µM ATP-G-actin, 10% labeled) was performed in the presence of different vimentin constructs. Wild-type vimentin (Vim^{WT}) and tailless vimentin ($Vim^{\Delta tail}$) assemble into filaments. Vim^{Y117L} assembles into unit-length-filaments (ULFs) that do not anneal end-to-end. Headless-vimentin ($Vim^{\Delta head}$) forms tetramers that do not assemble into filaments. The numbers represent the positions of the residues that delimit the head and tail domains. (*B*) Actin elongation rate increases in the presence of 18 µM of vimentin (1 mg/mL) under different oligomerization states: tetramers (+$Vim^{\Delta head}$), ULFs (+Vim^{Y117L}), or filamentous (+Vim^{WT}), compared to the average rate of the control condition for each replicate. Colors depict experiments performed on the same day. Small dots: individual elongation rate increases ($n \geq 20$ rates per replicate), large dots: average elongation rate increases of the replicates ($Vim^{\Delta head}$: $N = 8$, Vim^{Y117L}: $N = 6$, Vim^{WT}: $N = 11$ independent replicates), black bars: mean elongation rate increase computed from the replicate averages. The data shown for wild-type vimentin are the same as shown in Fig. 1*D*. (*C*) Actin elongation rate increases in the presence of 18 µM of Vim^{WT} (1 mg/mL) or $Vim^{\Delta tail}$ (0.85 mg/mL) assembled into filaments. Colors depict experiments performed on the same day. Small dots: individual elongation rate increases ($n \geq 20$ rates per replicate), large dots: average normalized elongation rates of the replicates ($N = 4$ independent replicates), black bars: mean elongation rate increase computed from the replicate averages. Experiments in *C* were conducted in the standard assembly buffer at 50 mM KCl. Statistical significance of the differences between conditions in *B* and *C* was evaluated by running two-tailed paired *t* tests over the replicate averages. $^*P < 0.05$, $^{**}P < 0.01$, $^{***}P < 0.001$, ns: not significant ($P > 0.05$). For *B* and *C*, the raw actin elongation rates are shown in *SI Appendix*, Fig. S6. (*D*) Actin elongation rate increase (Δv), compared to the average rate of the control condition (without Vim^{Y117L}) measured on the same day, as a function of Vim^{Y117L} concentration ($[Vim^{Y117L}]$). Small dots: average rate increase of individual replicates ($n \geq 20$ rates per replicate and condition), large dots: average of the replicates for each concentration ($1 \leq N \leq 8$ replicates per concentration). Dashed line: fit of the unbinned data with the binding model $\Delta v = \Delta v_{max}/(1 + K_d^{BE-ULF}/[Vim^{Y117L}])$, where the only unknown parameter K_d^{BE-ULF} characterizes the putative interaction between the actin barbed end and Vim^{Y117L} within ULFs (*SI Appendix, Theoretical Modeling*). The plateau value Δv_{max} is fixed to its mean value obtained from the ATP-G-actin on- and off-rate constants of the $N = 3$ replicates in Fig. 1*F*. The fit yields $K_d^{BE-ULF} = 1.1$ µM (0.06 mg/mL). Shaded area: error in the fitted elongation rate increase Δv due to uncertainties in its plateau Δv_{max}. We vary the plateau value Δv_{max} within the range given by its SE (SEM). This leads to a continuum of fitted curves, with values of K_d^{BE-ULF} in the range (0.4 to 2.1) µM.

Downloaded from https://www.pnas.org by Cecile Leduc on July 6, 2026 from IP address 81.194.28.6.

actin assembly. To address this question, we produced a truncated version of vimentin lacking the last 55 amino acids ($Vim^{\Delta tail}$) and performed the actin polymerization assay (Fig. 1*A*) in the presence of this mutant. This tailless vimentin mutant assembles into filaments (3, 49). $Vim^{\Delta tail}$ increased the actin elongation rate to the same extent as wild-type vimentin, with no significant difference between the two conditions (Fig. 3*C*), indicating that the tail domain is not required to promote actin elongation at the barbed end.

Vimentin Promotes Actin Filament Elongation in a Dose-Dependent Manner. We next investigated whether vimentin's effect depends on the vimentin concentration. To this end, we took advantage of the vimentin Y117L mutant, which allows for the precise control of both the number and oligomerization state of vimentin (ULFs). Actin polymerization assays were performed with 0.5 μM ATP-G-actin in the presence of Vim^{Y117L} ULFs at concentrations ranging from 0 to 22 μM of Vim^{Y117L} (0 to 1.18 mg/mL). The actin elongation rate difference relative to the control (Δv) increased with the vimentin Y117L concentration ($[Vim^{Y117L}]$) (Fig. 3*D*). As a first simple model, we propose that the saturation stems from a putative interaction between vimentin Y117L ULFs and the actin barbed end. In this framework, the barbed end of a growing actin filament is in a dynamic equilibrium between two states: free or occupied by a vimentin ULF (*SI Appendix, Theoretical Modeling*). Accordingly, our polymerization assay probes the ATP-G-actin on- and off-rate constants in the two extreme cases of this model where the barbed end is either never (Control) or always occupied (+Vim), implying that the effect saturates at a corresponding maximum value Δv_{max}. Thus, we model the increase in actin elongation rate by $\Delta v = \Delta v_{max}/(1 + K_d^{BE-ULF}/[Vim^{Y117L}])$, where the only unknown parameter K_d^{BE-ULF} characterizes the global interaction between actin barbed ends and vimentin within ULFs, and encompasses unresolved molecular details. Fitting this model to the dose-dependent acceleration of actin elongation by vimentin Y117L yields a dissociation constant of about 1.1 μM (0.06 mg/mL). Hence, the effect of vimentin on actin elongation reaches saturation with only a limited amount of vimentin, as compared to the physiological range [estimated to be >18 μM or 1 mg/mL in HeLa cells (51)].

Vimentin Promotes Actin Nucleation. Vimentin's effect on ATP-actin subunits at the barbed end significantly lowers the critical concentration for net ATP-actin elongation, defined as the ratio between the actin off-rate k_{off}^{ATP} and the on-rate k_{on}^{ATP}. We hypothesized that vimentin could also enhance the nucleation of actin filaments, which requires the formation of a critical nucleus, most commonly described as a tetramer, although some models suggest a trimer (52–54). Because small oligomers are unstable, their formation represents the principal barrier to nucleation. By stabilizing the interaction between ATP-actin subunits, vimentin could reduce this barrier and promote actin oligomerization to form a critical nucleus. To test this hypothesis, we first analyzed the ability of vimentin to nucleate actin filaments in the bulk using a pyrene fluorescence assay (Fig. 4*A*). The presence of vimentin decreased the initial lag time associated with actin filament nucleation, and fitting the polymerization curves at early times (*SI Appendix, Materials and Methods*) using the off-rate k_{off}^{ATP} and on-rate k_{on}^{ATP} constants extracted from previous experiments (Fig. 1*F*) revealed a ~35% increase in the initial nucleation rate (Fig. 4 *B*, *Left*; $4.9 \pm 1.3 \times 10^{-9}$ μM s^{-1} with vimentin vs. $3.6 \pm 0.9 \times 10^{-9}$ μM s^{-1} without vimentin, mean ± SD, $N = 3$ independent replicates). The differences in plateau intensity were also qualitatively consistent with the difference in critical elongation concentration we characterized. Fitting the slope of the polymerization curve at each time point further indicated that the actin barbed end concentration remains enhanced in the plateau regime (Fig. 4*C*). To support our empirical analysis, we propose a minimal theoretical model of F-actin nucleation and elongation subject to a limited monomer pool $c_0 = [ATP - G - actin](t = 0)$ (*SI Appendix, Theoretical Modeling*). We consider the nucleation of critical tetrameric F-actin nuclei with a rate constant k_{nucl}, and ATP-G-actin depletion due to polymerization with a rate constant k_{on}^{ATP}. We reason that short filaments tend to disassemble when the free ATP-G-actin concentration c is below the critical concentration for elongation $c_c = k_{off}^{ATP}/k_{on}^{ATP}$. As a result, nucleation events in this regime are typically unproductive and need not be considered in our formalism. We thus adopt an expression for the net nucleation rate $r_{nucl}(c)$ that vanishes at $c = c_c$, and satisfies the c^4 dependence at large actin concentrations consistent with tetrameric F-actin nuclei, $r_{nucl}(c) = k_{nucl}(c - c_c)^4$. This allows us to predict the number of actin barbed ends per unit volume as a function of time

$$n(t) = \frac{tanh\left(\sqrt{2}t/\tau\right)}{\sqrt{2}k_{on}^{ATP}\tau},$$

where we have defined the time scale $\tau = 1/\sqrt{k_{on}^{ATP} r_{nucl}(c_0)}$ over which ATP-G-actin is depleted. The only unknown parameter, namely the nucleation rate constant k_{nucl}, is fitted from the actin polymerization curve (*SI Appendix,* Fig. S7*B*), which allows us to compute the initial nucleation rate $r_{nucl}(c_0)$, confirming that this rate is increased by vimentin (Fig. 4 *B*, *Right*). The quantitative mismatch with the empirical analysis may result from assuming the same critical concentration for nucleation as for elongation. Also, the model does not take into account experimental variability in the actin on- and off-rates and how vimentin affects them. Nevertheless, the good agreement between the model and the empirical analysis in the number of barbed ends over time (Fig. 4*C*) corroborates that vimentin enhances both actin nucleation and elongation. Additional pyrene assays in the presence of profilin showed no effect of vimentin on the nucleation of actin filaments from profilin–G-actin complexes (*SI Appendix,* Fig. S3*C*), which is consistent with a model where vimentin would stabilize actin dimers and trimers, the formation of which is prevented by profilin. We then designed a fluorescence microscopy assay to directly visualize the nucleation of actin filaments. We mixed ATP-G-actin at low concentration (300 nM, 10% fluorescently labeled) in assembly buffer without or with preformed vimentin filaments, and confined the sample between two passivated glass coverslips, allowing us to detect and count filaments over time (Fig. 4*D*). We observed that the addition of vimentin filaments increased the number of actin filaments created by unit of time (Fig. 4*E*). Taken together, these results show that vimentin, beyond lowering the actin critical concentration for elongation, also accelerates filament formation, providing a direct mechanism by which vimentin intermediate filaments can modulate actin network assembly.

Vimentin Interacts Directly with Actin Monomers. The effect of vimentin on actin nucleation suggests the existence of a direct interaction between vimentin and actin monomers. To test this, we designed a pull-down assay in which varying amounts of vimentin wild-type filaments were immobilized on magnetic beads and used

Downloaded from https://www.pnas.org by Cecile Leduc on July 6, 2026 from IP address 81.194.28.6.

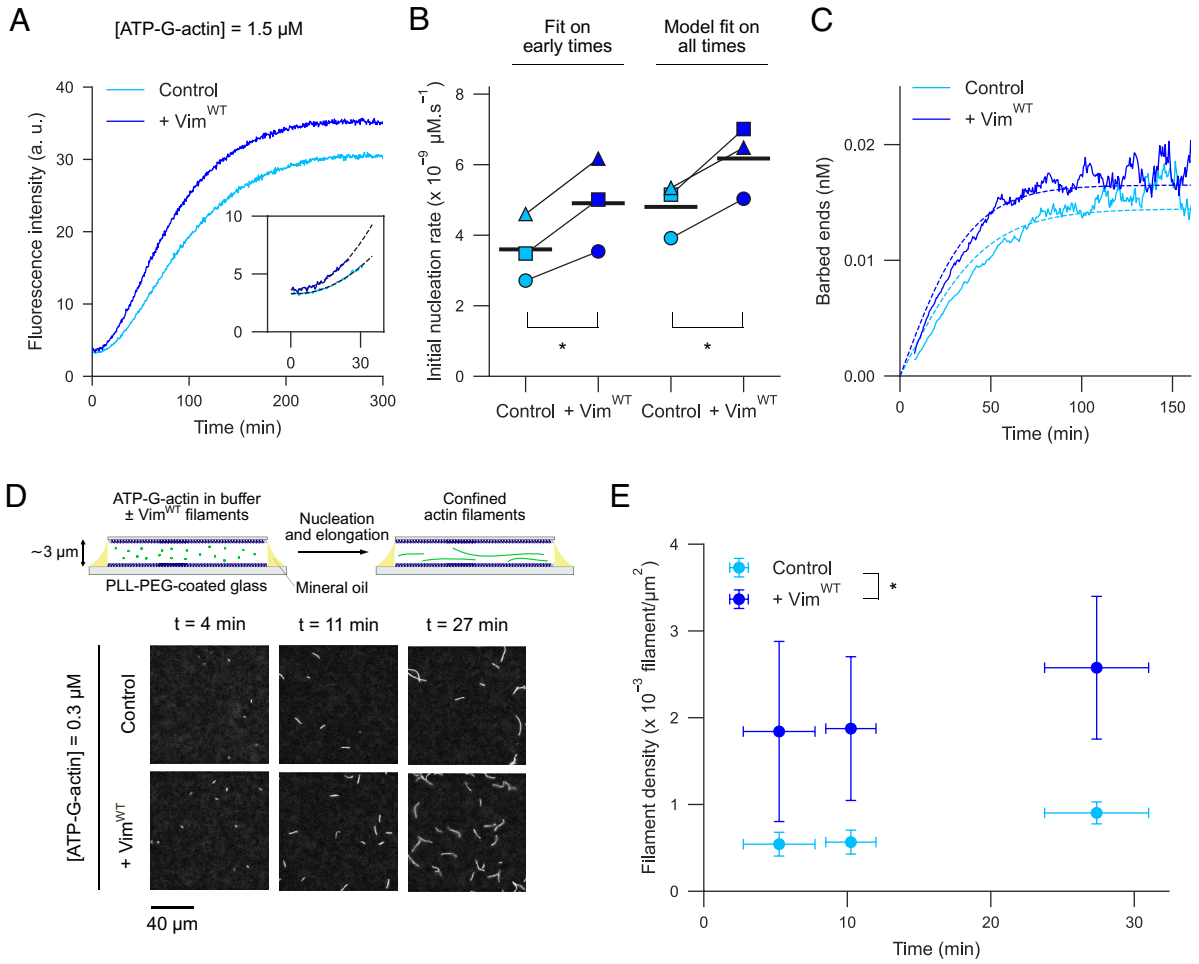


Fig. 4. Vimentin promotes actin nucleation. (*A*) Representative pyrene-actin fluorescence assay of actin assembly. Actin (1.5 µM, 8% pyrene-labeled) was assembled in the absence (Control, light blue) and in the presence of 18 µM wild-type vimentin (1 mg/mL) preassembled into filaments (+Vim^{WT}, dark blue). Raw fluorescence signals were corrected for the vimentin signal (*SI Appendix, Materials and Methods*). The *Inset* shows an enlarged plot of the early time points, which were first corrected for photobleaching (*SI Appendix,* Fig. S7*A*) and then fitted based on previously described method (55) to extract the initial nucleation rate (black dashed lines, see *SI Appendix, Materials and Methods*). This representative replicate corresponds to the one represented with squares in the quantification in *B*. (*B*) Quantification of the initial nucleation rate for $N = 3$ independent replicates in control (light blue) and vimentin (+Vim^{WT}, dark blue) conditions, using two different methods: empirical one-parameter fit on early time points as previously described (55) (*Left*), or one-parameter fit of the whole polymerization curve using our theoretical model (*Right*, and *SI Appendix*, Fig. S7*B*). Symbols: initial nucleation rates measured for each replicate with both methods, black bars: mean initial nucleation rates over the three replicates. Statistical significance of the difference between conditions was evaluated by running two-tailed paired *t* tests. *$P < 0.05$. (*C*) Concentration of actin barbed ends over time in the absence (Control, light blue) and in the presence of 18 µM wild-type vimentin (1 mg/mL) preassembled into filaments (+Vim^{WT}, dark blue), for the replicate shown in *A*. Plain curves: barbed end concentration computed from the rate of actin polymerization over time, given by the slope at each time point along the fluorescence curve (*SI Appendix, Materials and Methods*). Dashed lines: barbed end concentration predicted by our theoretical model described in the main text, following a one-parameter fit of the polymerized actin concentration over time (*SI Appendix*, Fig. S7*B* and *Theoretical Modeling*). (*D*) Direct visualization of actin nucleation by epifluorescence microscopy. (*Top*) schematic representation of the experiment. ATP-G-actin (0.3 µM, 10% labeled) was mixed in assembly buffer with or without preassembled wild-type vimentin filaments, and a small volume of the sample was confined between two passivated glass coverslips, resulting in a ~3-µm-high chamber. The chamber was sealed using mineral oil. (*Bottom*) Representative snapshots of nucleated actin filaments in the absence (Control) or in the presence of 18 µM wild-type vimentin (1 mg/mL) preassembled into filaments (+Vim^{WT}). (*E*) Quantification of the mean filament density in (*D*) as a function of time in control (light blue) and vimentin (+Vim^{WT}, dark blue) conditions. Each dot represents the mean ± SEM of $N = 4$ replicates for a time interval depicted by the horizontal error bar. For each replicate, condition, and time point, the mean number of filaments from $24 \leq n \leq 94$ fields of view was computed. Statistical significance of the difference between conditions was evaluated by running a two-way ANOVA. *$P < 0.05$.

to capture ATP-G-actin (Fig. 5*A*). Pellets and supernatants were analyzed by SDS-PAGE followed by gel staining, with known concentrations of actin and vimentin loaded on the same gel to generate calibration curves (Fig. 5*B*). We observed that the fraction of actin recovered in the pellet increased with the amount of vimentin on the beads (Fig. 5*C*). We fitted the fraction of actin specifically bound to the vimentin-coated beads (p) as a function of the free vimentin concentration in the pellet ($[Vim^{WT}_{free}]$) with the equation: $p = 1/(1 + K_d^{app}/[Vim^{WT}_{free}])$, where K_d^{app} is the apparent dissociation constant between filamentous vimentin and ATP-G-actin, when assuming a 1:1 binding stoichiometry between ATP-G-actin and vimentin monomers (Fig. 5*D* and *SI Appendix, Theoretical Modeling*). Pooling the data from five independent experiments allowed us to estimate K_d^{app} to be of the order of 6 µM vimentin monomers (0.3 mg/mL). This value should be considered approximate. First, actin in solution may not be strictly monomeric due to spontaneous nucleation, potentially leading to an underestimation of the apparent dissociation constant. Second, although our quantification method accounts for the nonspecific binding of actin to the beads, such binding may be reduced when beads are coated with vimentin, which would instead lead to an overestimation of the apparent dissociation constant. As we do not resolve the molecular details of the interaction, we analyzed

Downloaded from https://www.pnas.org by Cecile Leduc on July 6, 2026 from IP address 81.194.28.6.

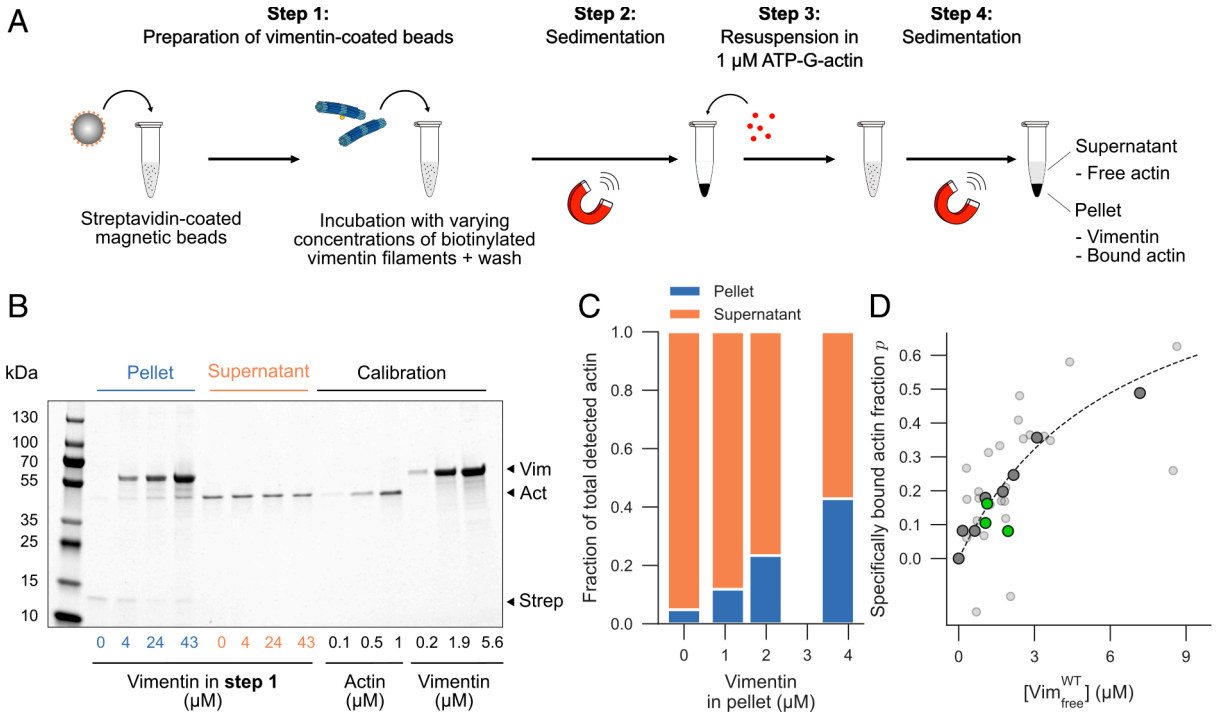


Fig. 5. Vimentin directly interacts with actin. (*A*) Actin–vimentin magnetic pull-down assay. In step 1, streptavidin-coated magnetic beads are incubated with varying concentrations of biotinylated vimentin filaments. In step 2, the beads are pulled with a magnet, and the supernatant containing unbound vimentin is discarded. The beads are further rinsed with a buffer to completely remove unattached vimentin. In step 3, the vimentin-coated beads are resuspended in a solution containing 1 μM ATP-G-actin, and immediately pulled down with the magnet (step 4). The protein content of the pellet and the supernatant is then analyzed by SDS-PAGE. Step 3 and 4 were performed in less than a minute, limiting possible actin nucleation. The experiment was performed in the standard assembly buffer. (*B*) Representative SDS-PAGE gel obtained with the assay described in A. Four concentrations of vimentin ranging from 0 to 43 μM (0 to 2.3 mg/mL) were used in step 1, and for each concentration, the pellet and supernatant obtained after step 4 were loaded. The six lanes on the right were loaded with samples containing known concentrations of actin or vimentin for calibration. Arrowheads indicate bands corresponding to vimentin (Vim), actin (Act), and streptavidin (Strep). The streptavidin band intensity provides a readout of the magnetic bead concentration. (*C*) Quantification of the electrophoresis gel shown in *B*. Fraction of total detected actin found in the pellet (blue) and in the supernatant (orange) as a function of the vimentin concentration measured in the pellet. (*D*) Fraction of available actin in solution specifically pulled with vimentin *(p)*, as a function of the free vimentin concentration in the pellet ($[Vim^{WT}_{free}]$). The amount of actin specifically bound to vimentin, as well as the amount of available actin in solution, was estimated by subtracting the amount of actin nonspecifically bound to the beads, and by taking into account the difference in bead concentration between conditions (*SI Appendix, Materials and Methods*). The free vimentin concentration is defined as the total vimentin concentration measured in the pellet, minus the concentration of vimentin bound to actin. The latter is equal to the concentration of specifically bound actin, if we assume a 1:1 stoichiometry to extract the apparent G-actin–vimentin dissociation constant K_d^{app}. Data collected from $N = 5$ independent experiments were pooled together (small light dots) and binned by $[Vim^{WT}_{free}]$ (large dark dots). Each bin contains four data points. The unbinned data were fitted (dashed line) to the equation: $p = 1/(1 + K_d^{app}/[Vim^{WT}_{free}])$. Green symbols represent data points obtained when adding 3 μM of profilin to the ATP-G-actin solution in Step 3.

the effect of different stoichiometries (*SI Appendix,* Fig. S8 and *Theoretical Modeling*). Comparison with the data provides a lower bound of five accessible binding sites per vimentin filament cross-section [~40 monomers (56)]. Additional experiments in the presence of profilin (1 μM G-actin, 3 μM profilin) showed that profilin–G-actin complexes cosediment with vimentin similarly to G-actin alone (Fig. 5*D*, green symbols). While the microscopic interaction remains unresolved, our data provide strong evidence for a direct and specific interaction between actin monomers and vimentin.

Discussion

In this work, we addressed the question of the direct interaction between actin and vimentin at the molecular level, providing insight into cytoskeletal crosstalk. Combining in vitro assays with theoretical modeling, we found that the sole presence of vimentin enhances actin nucleation and barbed end elongation by specifically stabilizing ATP-actin subunits, without interfering with the binding of additional monomers. Pull-down experiments confirmed a direct interaction between the two proteins. Together, our findings identify vimentin as an unexpected regulator of actin dynamics and highlight a mechanism by which intermediate filaments can directly influence actin networks.

Our results rule out macromolecular crowding as an explanation of vimentin's effect on actin dynamics. Previous in vitro studies using inert macromolecules have shown that macromolecular crowding can accelerate actin elongation, most likely due to excluded volume effects (57, 58). However, this effect requires concentrations of crowders typically above 20 mg/mL, a range we verified in our experimental conditions using Dextran (57, 58) (*SI Appendix*, Fig. S9*A*). At 20 mg/mL, the volume occupied by Dextran macromolecules (40 kDa) can be estimated to be around 15%, assuming spheres with a hydrodynamic radius of 5 nm (59). In contrast, the accelerating effect of vimentin occurs at much lower concentrations (~0.2 mg/mL, corresponding to 3.7 μM vimentin) and quickly saturates at higher vimentin concentrations (~1 mg/mL, corresponding to 18 μM vimentin). In this range, the volume excluded by vimentin remains negligible (<0.5%) and cannot account for the observed acceleration. Moreover, the mechanism we uncovered—stabilization of ATP-actin at the barbed end through a decrease in the off-rate while leaving the on-rate unaffected—is fundamentally different from the effect of inert crowders. Indeed, the acceleration of actin elongation by these

Downloaded from https://www.pnas.org by Cecile Leduc on July 6, 2026 from IP address 81.194.28.6.

macromolecular crowders is dominated by an increase in the on-rate, which can be interpreted as an increase in the effective monomer concentration (58) (*SI Appendix*, Fig. S9*B*). Finally, if excluded volume effects had a significant contribution to vimentin's effect, one would expect vimentin's effect to be independent of actin nucleotide state, and to observe the same acceleration for ADP-actin polymerization, which we did not observe. Altogether, these three observations–the low vimentin concentrations at which its effect occurs, the demonstrated stabilizing mechanism, and the dependency on actin nucleotide state–argue strongly against a role of crowding.

The specific stabilization of ATP-actin but not ADP-actin subunits at filament barbed ends by vimentin is an intriguing result. One possible explanation for this nucleotide dependence could be a difference in the accessibility of actin residues which can interact with vimentin. So far, only the structure of the barbed end with a terminal actin subunit in the ADP-state, which is in an F-actin conformation, has been obtained (60, 61). One can speculate that, during elongation, the recently added terminal subunit in the ATP-state could transiently remain in a G-actin-like conformation, which could thus allow it to interact with vimentin as supported by our pull-down assay. A second possible explanation for this nucleotide dependence is suggested by our observation that vimentin changes the critical concentration for actin elongation, and what this observation implies thermodynamically. Indeed, thermodynamics forbids the mere equilibrium binding of a protein with the filament barbed end from modifying this concentration, even though it can dramatically affect the individual on- and off-rate constants as long as their ratio remains unchanged. Thus, the change in the critical concentration induced by vimentin implies that vimentin's effect operates out of equilibrium, which could be explained by a coupling of vimentin binding to the nucleotide dynamics, among other possible mechanisms.

The domain(s) of vimentin implicated in its effect on actin elongation remain unknown, although we ruled out the implication of vimentin head and tail domains in the experiments using truncated constructs. Mapping the potential interaction sites, for example, by systematic point mutation within the rod domain, crosslinking, or using structural approaches, would be critical to understand the actin–vimentin binding interface and how vimentin specifically stabilizes ATP-actin subunits at the barbed end. While vimentin could in principle bind along the actin filament and induce allosteric effects at the barbed end, the weak nature of the interaction makes it unlikely to propagate beyond a few subunits. Additionally, such an effect would need to differentially affect the barbed end depending on whether actin is ATP- or ADP-bound. Cryogenic electron microscopy has been instrumental in understanding the mechanisms involved in actin assembly (41, 61, 62) and how it is regulated by actin-binding proteins at the barbed end (60, 63–65). Similar high-resolution structural approaches applied to F-actin and vimentin are required to confirm if vimentin filaments interact with the barbed end, and if so, if they act by creating additional bonds between actin subunits at the barbed end or by modulating their conformation.

We quantified two dissociation constants: one characterizing the vimentin/ATP-G-actin interaction (Fig. 5*D*) and one characterizing a putative interaction between vimentin ULFs and actin barbed ends (Fig. 3*D*). However, it is difficult to compare these two dissociation constants quantitatively, as we do not resolve the involved microscopic interactions, which might differ between the two cases. Notably, the actin subunits at the barbed end and G-actin monomers expose distinct surface residues. Furthermore, the putative interaction between barbed ends and vimentin ULFs may involve multiple binding sites, possibly with some cooperativity.

Interestingly, recent in vitro studies demonstrated that vimentin stabilizes dynamic microtubules (66). The authors related this effect to a weak and transient microtubule–vimentin interaction, which they measured using optical tweezers. This interaction is sufficient to have a stabilization effect on microtubule dynamics without inducing coalignment or bundling between the two filament types. Similarly, we propose that frequent but transient interactions of vimentin in the vicinity of the barbed end of actin filaments underlie the stabilizing effect that we have characterized. In contrast to its effect on actin, vimentin does not increase the microtubule elongation rate, but instead decreases the catastrophe frequency and increases the rescue frequency. The differences between vimentin's effect on microtubules and on actin may arise from their distinct architectures and assembly pathways, although the underlying molecular mechanisms could be similar. However, because the study of the dynamic instability requires microtubules assembled from GTP–tubulin, the dependence of vimentin's effect on the tubulin nucleotide state could not be directly assessed. Together, these findings suggest that vimentin may act as a broad modulator of cytoskeletal turnover.

Vimentin differs from canonical actin barbed end regulators such as formins and Ena/VASP. These actin-binding proteins promote actin elongation through enhanced recruitment of (profilin-)actin monomers, thus having a major impact on the apparent actin on-rate (67–69). In contrast, vimentin does not significantly increase the recruitment of monomers but instead stabilizes the barbed end in the range of actin concentrations we tested. This suggests that vimentin does not act as a dominant driver of actin polymerization, such as formin and Ena/VASP, but may rather provide a layer of fine-tuning that contributes to cytoskeletal remodeling in regions where vimentin, actin filaments, and regulatory factors converge. In cells, where the concentration of actin monomers is typically at least one order of magnitude higher than in our in vitro assay, the direct contribution of the off-rate reduction to actin elongation velocities may therefore be limited. However, the fact that vimentin directly impacts the barbed end raises the possibility that it could modulate the activity of actin-binding proteins by acting synergistically or antagonistically with canonical barbed-end regulators. Future work should test whether vimentin synergizes or competes with other actin regulators and how cross-linkers or signaling pathways could further tune this effect in cells.

Materials and Methods

Detailed protocols are included in the *SI Appendix*. We purified recombinant wild-type human vimentin and vimentin mutants from *Escherichia coli* (8, 9, 37). Vimentin was stored as denatured monomers in 8 M urea at −70 °C. Prior to experiments, vimentin was renatured by stepwise dialysis to sodium phosphate buffer (pH 7.0, 2.5 mM sodium phosphate, 1 mM DTT), leading to the formation of tetramers. Vimentin filaments were assembled in a buffer compatible with actin assembly (assembly buffer: 10 mM HEPES pH 7.0, 1 mM sodium phosphate, 1 mM $MgCl_2$, 0.2 mM EGTA, 100 mM KCl). KCl was added at the last minute to start vimentin filament assembly. The vimentin mix, typically at 1 mg/mL, was then incubated at 37 °C for 30 min. 1 mg/mL of vimentin corresponds to 4.7 μM of vimentin tetramers, and 18.6 μM of vimentin monomers. We followed the same steps for experiments with vimentin Y117L and vimentin Δhead. The assembly protocol had to be optimized for vimentin Δtail to prevent the formation of unwanted aggregates. Vimentin Δtail filaments were assembled in a modified assembly buffer (10 mM HEPES, pH 7.0, 1 mM sodium phosphate, 1 mM DTT, 0.2 mM EGTA, 50 mM KCl), supplemented with 1 mM $MgCl_2$ just before introducing the sample into the flow chamber. For ADP-actin polymerization experiments in Tris

Downloaded from https://www.pnas.org by Cecile Leduc on July 6, 2026 from IP address 81.194.28.6.

buffer, vimentin dialyzed in Tris dialysis buffer (5 mM Tris-HCl pH 8.0, 1 mM DTT) was prepared in Tris assembly buffer (10 mM Tris-HCl, pH 7.0 at 37 °C, 1 mM $MgCl_2$, 0.2 mM EGTA, 50 mM KCl). The vimentin mix was then incubated at 37 °C for 1 h.

Alpha skeletal actin was purified from rabbit muscle and stored in G-buffer (2 mM Tris-HCl, pH 7.8, 1 mM DTT, 0.2 mM $CaCl_2$, 0.2 mM ATP, 0.01% NaN_3) (37, 40). Actin was labeled with Alexa Fluor (AF)-488, Atto-643, or Atto-488 NHS Ester.

Polymerization and depolymerization experiments in TIRF microscopy were performed in flow chambers made of two cleaned glass coverslips (22 × 40 mm, #1.5, VWR) silanized with dichlorodimethylsilane. The flow chamber was first coated with neutrAvidin at 10 μg/mL for 5 min and rinsed with the assembly buffer. The surfaces were then passivated by incubation of Pluronic F127 1% for 15 min, thoroughly rinsed with the assembly buffer, and further passivated with bovine serum albumin (BSA) at 10 mg/mL for 5 min. Both F127 and BSA solutions were diluted in the assembly buffer. Biotinylated F-actin fragments were prepared by preassembly of F-actin (10% Atto-643-labeled, 10% biotinylated) in a test tube at 10 μM for 1 h at room temperature (in G-buffer supplemented with 100 mM KCl), followed by a 1:500 dilution in assembly buffer containing Atto-643-labeled ATP-G-actin (nonbiotinylated) at 0.2 μM to prevent depolymerization. The actin filaments were finally fragmented by strong pipetting and introduced into the flow chamber for a few seconds. The chamber was rinsed with the assembly buffer containing 0.2 μM Atto-643-labeled ATP-G-actin to remove unbound filaments. The polymerization experiment was then started by flowing 10% AF 488 or Atto 488-labeled, 0.15% biotinylated ATP-G-actin in the assembly buffer (except for ADP-G-actin polymerization) supplemented with 0.2 mM ATP, as well as 1 mM DTT, 1.2 mg/mL glucose, 40 μg/mL glucose oxidase, and 8 μg/mL catalase used as oxygen scavengers to limit photobleaching and creation of reactive oxygen species. The ADP-G-actin polymerization assay was performed in the Tris assembly buffer, supplemented with 1 mM DTT and the oxygen scavengers. Observations were carried out on an inverted microscope (Nikon Eclipse Ti), using TIRF (Ilas 2 system, Gataca systems) or wide field microscopy with a 60× objective NA 1.49. Images were acquired by a Kinetix camera (Teledyne Photometrics). The experiment was controlled using MicroManager. Movies were analyzed using TSOAX (38).

Data, Materials, and Software Availability. Study data are included in the article and/or supporting information.

ACKNOWLEDGMENTS. We thank the Romet-Lemonne/Jegou lab for assistance and exciting discussions and specifically Ingrid Billault-Chaumartin for careful reading of the manuscript. We thank Sarah Köster and Peter Bieling for sharing plasmids. C.L. thanks Harald Herrmann and Tatjana Wedig for teaching her vimentin purification, and the support of the EU-supported Cooperation in Science and Technology action NANONET. This project was funded by "Investissements d'Avenir" Labex WhoAmI? (ANR-11-LABX-0071) and the Université Paris Cité IdEx (ANR-IDEX-0001), the Agence Nationale pour la recherche (ANR-21-CE11-0004-02), the Impulscience program of Fondation Bettencourt-Schueller and the Centre National de la Recherche Scientifique. L.P. was funded by La Ligue contre le Cancer (LNCC 282810).

Author affiliations: [a]Université Paris Cité, CNRS, Institut Jacques Monod, Paris F-75013, France; [b]Université Paris-Saclay, CNRS, Laboratoire de Physique Théorique et Modèles Statistiques, Orsay F-91405, France; and [c]Physique et Mécanique des Milieux Hétérogènes, CNRS, Ecole Supérieure de Physique et de Chimie Industrielles de la Ville de Paris, Paris Science et Lettres Research University, Sorbonne Université, Université Paris Cité, Paris F-75005, France

Author contributions: L.P., A.J., G.R.-L., and C.L. designed research; L.P., L.K., M.V.-S., Q.D.T., and C.L. performed research; L.P., L.K., M.V.-S., and M.L. contributed new reagents/analytic tools; L.P. analyzed data; L.K. and M.L. theoretical modeling; and L.P., L.K., and C.L. wrote the paper.

1. J. E. Eriksson *et al.*, Introducing intermediate filaments: From discovery to disease. *J. Clin. Invest.* **119**, 1763–1771 (2009).
2. C. Leduc, S. Etienne-Manneville, Intermediate filaments in cell migration and invasion: The unusual suspects. *Curr. Opin. Cell Biol.* **32**, 102–112 (2015).
3. H. Herrmann, U. Aebi, Intermediate filaments: Structure and assembly. *Cold Spring Harb. Perspect. Biol.* **8**, a018242 (2016).
4. S. Etienne-Manneville, Cytoplasmic intermediate filaments in cell biology. *Annu. Rev. Cell Dev. Biol.* **34**, 1–28 (2018).
5. R. A. Battaglia, S. Delic, H. Herrmann, N. T. Snider, Vimentin on the move: New developments in cell migration. *F1000Research* **7**, 1796 (2018).
6. K. M. Ridge, J. E. Eriksson, M. Pekny, R. D. Goldman, Roles of vimentin in health and disease. *Genes Dev.* **36**, 391–407 (2022).
7. C. Hookway *et al.*, Microtubule-dependent transport and dynamics of vimentin intermediate filaments. *Mol. Biol. Cell* **26**, 1675–1686 (2015).
8. Q. D. Tran *et al.*, Continuous self-repair protects vimentin intermediate filaments from fragmentation. *Proc. Natl. Acad. Sci. U.S.A.* **122**, e2417660122 (2025).
9. Q. D. Tran, V. Sorichetti, G. Pehau-Arnaudet, M. Lenz, C. Leduc, Fragmentation and entanglement limit vimentin intermediate filament assembly. *Phys. Rev. X* **13**, 011014 (2023).
10. F. Alisafaei *et al.*, Vimentin is a key regulator of cell mechanosensing through opposite actions on actomyosin and microtubule networks. *Commun. Biol.* **7**, 658 (2024).
11. S. Duarte *et al.*, Vimentin filaments interact with the actin cortex in mitosis allowing normal cell division. *Nat. Commun.* **10**, 1–19 (2019).
12. B. Eckes *et al.*, Impaired mechanical stability, migration and contractile capacity in vimentin deficient fibroblasts. *J. Cell Sci.* **111**, 1897–1907 (1998).
13. M. P. Serres *et al.*, F-actin interactome reveals vimentin as a key regulator of actin organization and cell mechanics in mitosis. *Dev. Cell* **52**, 210–222 (2020).
14. F. Huber, A. Boire, M. P. López, G. H. Koenderink, Cytoskeletal crosstalk: When three different personalities team up. *Curr. Opin. Cell Biol.* **32**, 39–47 (2015).
15. S. Seetharaman, S. Etienne-Manneville, Cytoskeletal crosstalk in cell migration. *Trends Cell Biol.* **30**, 720–735 (2020).
16. L. Pradeau-Phélut, S. Etienne-Manneville, Cytoskeletal crosstalk: A focus on intermediate filaments. *Curr. Opin. Cell Biol.* **87**, 102325 (2024).
17. E. J. van Bodegraven, S. Etienne-Manneville, Intermediate filaments against actomyosin: The david and goliath of cell migration. *Curr. Opin. Cell Biol.* **66**, 79–88 (2020).
18. Y. Jiu *et al.*, Bidirectional interplay between vimentin intermediate filaments and contractile actin stress fibers. *Cell Rep.* **11**, 1511–1518 (2015).
19. Y. Jiu *et al.*, Vimentin intermediate filaments control actin stress fiber assembly through GEF-H1 and RhoA. *J. Cell Sci.* **130**, 892–902 (2017).
20. X. Huang *et al.*, Vimentin intermediate filaments coordinate actin stress fibers and podosomes to determine the extracellular matrix degradation by macrophages. *Dev. Cell* **60**, 1669–1685.e6 (2025).
21. N. Costigliola *et al.*, Vimentin fibers orient traction stress. *Proc. Natl. Acad. Sci. U.S.A.* **114**, 5195–5200 (2017).
22. J. P. Conboy, M. G. Lettinga, P. E. Boukany, F. C. MacKintosh, G. H. Koenderink, Actin and vimentin jointly control cell viscoelasticity and compression stiffening. bioRxiv [Preprint] (2025). https://doi.org/10.1101/2025.01.01.630993 (Accessed 10 October 2025).
23. J. Hu *et al.*, High stretchability, strength, and toughness of living cells enabled by hyperelastic vimentin intermediate filaments. *Proc. Natl. Acad. Sci. U.S.A.* **116**, 17175–17180 (2019).
24. A. Basu *et al.*, Vimentin undergoes liquid–liquid phase separation to form droplets which wet and stabilize actin fibers. *Proc. Natl. Acad. Sci. U.S.A.* **122**, e2418624122 (2025).
25. P. González-Jiménez *et al.*, Vimentin single cysteine residue acts as a tunable sensor for network organization and as a key for actin remodeling in response to oxidants and electrophiles. *Redox Biol.* **64**, 102756 (2023).
26. H. Wu *et al.*, Vimentin intermediate filaments and filamentous actin form unexpected interpenetrating networks that redefine the cell cortex. *Proc. Natl. Acad. Sci. U.S.A.* **119**, e2115217119 (2022).
27. P. J. Hollenbeck, A. D. Bershadsky, O. Y. Pletjushkina, I. S. Tint, J. M. Vasiliev, Intermediate filament collapse is an ATP-dependent and actin-dependent process. *J. Cell Sci.* **92**, 621–631 (1989).
28. A. Robert, H. Herrmann, M. W. Davidson, V. I. Gelfand, Microtubule-dependent transport of vimentin filament precursors is regulated by actin and by the concerted action of Rho- and p21-activated kinases. *FASEB J.* **28**, 2879–2890 (2014).
29. C. Leduc, S. Etienne-Manneville, Regulation of microtubule-associated motors drives intermediate filament network polarization. *J. Cell Biol.* **216**, 1689–1703 (2017).
30. A. S. Menko *et al.*, A central role for vimentin in regulating repair function during healing of the lens epithelium. *Mol. Biol. Cell* **25**, 776–790 (2014).
31. S. Osmanagic-Myers *et al.*, Plectin reinforces vascular integrity by mediating vimentin–actin network crosstalk. *J. Cell Sci.* **128**, 4138–4150 (2015).
32. I. Correia, D. Chu, Y.-H. Chou, R. D. Goldman, P. Matsudaira, Integrating the actin and vimentin cytoskeletons: Adhesion-dependent formation of fimbrin-vimentin complexes in macrophages. *J. Cell Biol.* **146**, 831–842 (1999).
33. H. Kim *et al.*, Filamin A is required for vimentin-mediated cell adhesion and spreading. *Am. J. Physiol. Cell Physiol.* **298**, C221–C236 (2010).
34. O. Esue, A. A. Carson, Y. Tseng, D. Wirtz, A direct interaction between actin and vimentin filaments mediated by the tail domain of vimentin. *J. Biol. Chem.* **281**, 30393–30399 (2006).
35. Y. Shen *et al.*, Effects of vimentin intermediate filaments on the structure and dynamics of in vitro multicomponent interpenetrating cytoskeletal networks. *Phys. Rev. Lett.* **127**, 108101 (2021).
36. T. Golde *et al.*, Glassy dynamics in composite biopolymer networks. *Soft Matter* **14**, 7970–7978 (2018).
37. I. I. Petitjean *et al.*, Reconstitution of cytolinker-mediated crosstalk between actin and vimentin. *Eur. J. Cell Biol.* **103**, 151403 (2024).
38. T. Xu *et al.*, Automated tracking of biopolymer growth and network deformation with TSOAX. *Sci. Rep.* **9**, 1717 (2019).
39. I. Fujiwara, D. Vavylonis, T. D. Pollard, Polymerization kinetics of ADP- and ADP-Pi-actin determined by fluorescence microscopy. *Proc. Natl. Acad. Sci. U.S.A.* **104**, 8827–8832 (2007).
40. A. Jégou *et al.*, Individual actin filaments in a microfluidic flow reveal the mechanism of ATP hydrolysis and give insight into the properties of profilin. *PLoS Biol.* **9**, e1001161 (2011).
41. W. Oosterheert, B. U. Klink, A. Belyy, S. Pospich, S. Raunser, Structural basis of actin filament assembly and aging. *Nature* **611**, 374–379 (2022).
42. L. Blanchoin, T. D. Pollard, Hydrolysis of ATP by polymerized actin depends on the bound divalent cation but not profilin. *Biochemistry* **41**, 597–602 (2002).
43. R. Cooke, Role of the bound nucleotide in the polymerization of actin. *Biochemistry* **14**, 3250–3256 (1975).

Downloaded from https://www.pnas.org by Cecile Leduc on July 6, 2026 from IP address 81.194.28.6.

44. T. D. Pollard, Polymerization of ADP-actin. *J. Cell Biol.* **99**, 769–777 (1984).
45. P. Bieling *et al.*, WH2 and proline-rich domains of WASP-family proteins collaborate to accelerate actin filament elongation. *EMBO J.* **37**, 102–121 (2018).
46. J. Funk *et al.*, Profilin and formin constitute a pacemaker system for robust actin filament growth. *Elife* **8**, e50963 (2019).
47. V. Prahlad, M. Yoon, R. D. Moir, R. D. Vale, R. D. Goldman, Rapid movements of vimentin on microtubule tracks: Kinesin-dependent assembly of intermediate filament networks. *J. Cell Biol.* **143**, 159–170 (1998).
48. P. Soellner, R. A. Quinlan, W. W. Franke, Identification of a distinct soluble subunit of an intermediate filament protein: Tetrameric vimentin from living cells. *Proc. Natl. Acad. Sci. U.S.A.* **82**, 7929–7933 (1985).
49. H. Herrmann *et al.*, Structure and assembly properties of the intermediate filament protein vimentin: The role of its head, rod and tail domains. *J. Mol. Biol.* **264**, 933–953 (1996).
50. M. Meier *et al.*, Vimentin coil 1A–A molecular switch involved in the initiation of filament elongation. *J. Mol. Biol.* **390**, 245–261 (2009).
51. D. B. Bekker-Jensen *et al.*, An optimized shotgun strategy for the rapid generation of comprehensive human proteomes. *Cell Syst.* **4**, 587–599.e4 (2017).
52. D. Sept, J. A. McCammon, Thermodynamics and kinetics of actin filament nucleation. *Biophys. J.* **81**, 667–674 (2001).
53. L. S. Tobacman, E. D. Korn, The kinetics of actin nucleation and polymerization. *J. Biol. Chem.* **258**, 3207–3214 (1983).
54. A. D. Rosenbloom, E. W. Kovar, D. R. Kovar, L. M. Loew, T. D. Pollard, Mechanism of actin filament nucleation. *Biophys. J.* **120**, 4399–4417 (2021).
55. L. K. Doolittle, M. K. Rosen, S. B. Padrick, "Measurement and Analysis of in vitro actin polymerization" in *Adhesion Protein Protocols*, A. S. Coutts, Ed. (Humana Press, 2013), pp. 273–293.
56. M. Eibauer *et al.*, Vimentin filaments integrate low-complexity domains in a complex helical structure. *Nat. Struct. Mol. Biol.* **31**, 939–949 (2024).
57. D. Drenckhahn, T. D. Pollard, Elongation of actin filaments is a diffusion-limited reaction at the barbed end and is accelerated by inert macromolecules. *J. Biol. Chem.* **261**, 12754–12758 (1986).
58. R. A. Lindner, G. B. Ralston, Macromolecular crowding: Effects on actin polymerisation. *Biophys. Chem.* **66**, 57–66 (1997).
59. J. K. Armstrong, R. B. Wenby, H. J. Meiselman, T. C. Fisher, The hydrodynamic radii of macromolecules and their effect on red blood cell aggregation. *Biophys. J.* **87**, 4259–4270 (2004).
60. P. J. Carman, K. R. Barrie, G. Rebowski, R. Dominguez, Structures of the free and capped ends of the actin filament. *Science* **380**, 1287–1292 (2023).
61. W. Oosterheert *et al.*, Molecular mechanisms of inorganic-phosphate release from the core and barbed end of actin filaments. *Nat. Struct. Mol. Biol.* **30**, 1774–1785 (2023).
62. S. Z. Chou, T. D. Pollard, Mechanism of actin polymerization revealed by cryo-EM structures of actin filaments with three different bound nucleotides. *Proc. Natl. Acad. Sci. U.S.A.* **116**, 4265–4274 (2019).
63. W. Oosterheert *et al.*, Molecular mechanism of actin filament elongation by formins. *Science* **384**, eadn9560 (2024).
64. J. Funk *et al.*, A barbed end interference mechanism reveals how capping protein promotes nucleation in branched actin networks. *Nat. Commun.* **12**, 5329 (2021).
65. N. J. Palmer, K. R. Barrie, R. Dominguez, Mechanisms of actin filament severing and elongation by formins. *Nature* **632**, 437–442 (2024).
66. L. Schaedel, C. Lorenz, A. V. Schepers, S. Klumpp, S. Köster, Vimentin intermediate filaments stabilize dynamic microtubules by direct interactions. *Nat. Commun.* **12**, 3799 (2021).
67. D. Breitsprecher *et al.*, Molecular mechanism of Ena/VASP-mediated actin-filament elongation. *EMBO J.* **30**, 456–467 (2011).
68. N. Courtemanche, J. L. Henty-Ridilla, Actin filament dynamics at barbed ends: New structures, new insights. *Curr. Opin. Cell Biol.* **90**, 102419 (2024).
69. S. Romero *et al.*, Formin is a processive motor that requires profilin to accelerate actin assembly and associated ATP hydrolysis. *Cell* **119**, 419–429 (2004).

Downloaded from https://www.pnas.org by Cecile Leduc on July 6, 2026 from IP address 81.194.28.6.